Quantized-Input Control Lyapunov Approach for Permanent Magnet Synchronous Motor Drives

Gideon Prior and Miroslav Krstic

Abstract—We present a new method for the generation of input switching sequences in a synchronous motor control system based on the evaluation of a control Lyapunov function over a discrete set of realizable inputs. Typical reference input realization methods, such as space vector modulation, rely on high-frequency state space averaging which can yield unnecessary switching events and increased switching losses. Alternative input selection strategies, such as lookup-table-based direct torque control, rely on heuristically chosen hysteresis bands to determine switching instants, which often results in a suboptimal choice between switching frequency and other performance measures. In this paper, we use an energy-related Lyapunov function to guide the input selection process by making switching decisions based on the stabilizing effect each input has on the closed-loop system. We provide a theoretical analysis of a motor–inverter system, leading to a stability proof for a quantized input control law. The controller performance is verified through computer simulations and experimental results.

Index Terms—Control Lyapunov methods, direct torque control, field-oriented control (FOC), motor drives, permanent magnet synchronous motor (PMSM), power electronics, quantized input systems, voltage fed inverters.

I. INTRODUCTION

HIGH-TORQUE permanent magnet synchronous motors (PMSMs) are becoming an increasingly popular choice in low to medium speed industrial motor applications where torque density and efficiency are critical. In comparison with induction motors, permanent magnet machines typically have lower inductance and a greater number of poles, yielding a small electrical time constant which leads control designers toward high-frequency commutation solutions as a means to generate sufficiently smooth stator currents. However, as the phase currents become large, as is typical in low-speed high-power applications, the maximum attainable switching frequency shrinks as a result of the thermal limitations of the switching elements. Thus, the control engineer is faced with the problem of maximizing the closed-loop performance of the system using a highly constrained actuator. This paper presents a conceptually simple field-oriented control (FOC) algorithm with intrinsic commutation that is capable

G. Prior is with the Department of Electrical and Computer Engineering, University of California, San Diego, CA 92093 USA (e-mail: gprior@ucsd.edu).

M. Krstic is with the Cymer Center for Control Systems and Dynamics, Department of Mechanical and Aerospace Engineering, University of California, San Diego, CA 92093 USA (e-mail: krstic@ucsd.edu).

Color versions of one or more of the figures in this paper are available online at http://ieeexplore.ieee.org.

of minimizing switching events while providing fast dynamic response, robustness to parametric uncertainty, and stability guarantees.

Being a fairly mature field, myriad techniques have been proposed over the years to improve the performance and efficiency of electric machines. Possibly the most notable of these is based on FOC first proposed in [1] and further detailed in [2]. FOC allowed controllers to be developed similar to well-established techniques applied to separately excited dc motors by attaching a rotating reference frame to the rotor via the Park transform. Once posed in this reference frame, trigonometric nonlinearities are removed, resulting in a bilinear system that allows for independent regulation of torque-producing and magnetizing currents. Now, in dealing with dc quantities, proportional plus integral (PI) feedback loops are used for regulation, which would otherwise have trouble tracking sinusoidal references.

Many researchers have proposed improvements to field-oriented control. Extended state observers (ESOs) have been developed for motor control applications to compensate for unmodeled dynamics and disturbances [3], [4], including the use of ESOs to enable the use of active disturbance rejection control in passivity-based designs [5]. In [6], the authors model the nonideal characteristics of a PMSM responsible for producing torque ripple and build an adaptive current controller nested inside a linear speed loop to minimize the non-dc components of the generated torque. A similar approach is shown in [7], where converter dynamics is included in addition to the Fourier series-based model of the torque spectra. Adaptive output feedback controllers have also been developed for classes of synchronous motors where the states to be controlled do not coincide with the measurable outputs [8]. Other nonlinear methods based on control Lyapunov functions have been reported in [9], as well as the related adaptive backstepping technique [10]–[13], which includes experimental comparisons between adaptive backstepping and robust control. These methods have been further refined in [14], where the authors design a continuous controller that achieves asymptotic tracking of a nonlinear system through the use of adaptive backstepping to address parametric uncertainties while employing a robust control technique to compensate for additive disturbances.

Field-oriented controllers are used to generate idealized continuous reference vectors and rely on standard pulse width modulation (PWM) techniques such as sine triangle PWM (ST-PWM) or space vector modulation (SVM) to approximate the desired input via high-speed switching. The design and optimization of switching methods has been widely studied and continues to be an active area of research [15], [16].

In [17], the authors exploit the nonuniqueness of the standard SVM switching sequence to subdivide switching regions in a way to determine the best available sequence for torque ripple minimization. In [18], a variation on the ST-PWM technique is presented where the carrier frequency is modulated by the slope of the modulator, yielding a dynamic switching frequency with fewer commutations on average. The need for advanced control of power electronic converters is not limited to motor drives, but rather applies to a wide class of systems requiring energy conversion. Backstepping techniques for PWM control are explored in [19], where the authors, through the use of state space averaging, formulate an expression for the duty cycle of a switch that drives the desired current and voltage from a photovoltaic array to target values determined by an extremum-seeking algorithm in order to maximize output power. Other improvements to standard FOC employ variable sampling techniques [20], randomized PWM [21]–[23], and online parameter estimation [24], which have been developed to address design specific objectives.

A popular alternative to FOC+PWM is direct torque control (DTC). As first described in [25], DTC does not compute reference vectors in the dq space for tracking, but instead uses hysteresis bands and a switching lookup table to keep estimates of the stator flux and the impressed torque in bounds. DTC has fast dynamic response and notably faster flux control capabilities when compared to FOC [26], [27], but can suffer from increased torque ripple and high switching losses depending on the size of the hysteresis bands [17], [28]. To mitigate these drawbacks, in [29] the use of multiple time scale control laws has been proposed to slow down system trajectories near switching surfaces, while others have proposed augmenting DTC with model predictive control (MPC) to optimize competing switching signals over a finite horizon [28], [30]–[32].

In this paper, we incorporate a model of a PMSM in the dq space and propose a control Lyapunov plus backstepping approach that provides stability guarantees. We then extend the proposed control law to govern the switching sequence of a class of quantized input systems. Rather than using continuous reference inputs and state-space averaging assumptions as used in PWM generation, we use stability information from a control Lyapunov function (CLF) evaluated at each input to select the switching configuration of the inverter, thus preserving the stability guarantees given by the continuous controller. Given more than one stabilizing input, it is possible to design input selection rules that minimize switching losses, randomize the switching spectra, or maximize dynamic response.

The rest of this paper is organized as follows. In Section II, we present the nonlinear model of a PMSM in the dq coordinate system. In Section III, we develop a continuous speed controller using the integrator backstepping method. The model of the inverter used to generate realizable inputs is given in both stationary and rotating reference frames in Section IV. In Section V, we derive the quantized input control law and discuss various methods of switching sequence optimization. Section VI contains simulation results, including speed and current regulation as well as a visualization of the input selection process. The controller performance and implementation feasibility are verified experimentally in Section VII. Section VIII provides a summary and some concluding remarks.

II. MODEL OF A PMSM IN THE dq REFERENCE FRAME

Using Kirchoff's voltage law and Newton's second law in rotational form, a PMSM motor model can be derived and transformed into the standard direct and quadrature field-oriented rotating reference frame [2]. The dq frame model of a PMSM is given as

$$\frac{di_d}{dt} = \frac{v_d}{L_d} - \frac{R}{L_d}i_d + p\omega_r \frac{L_q}{L_d}i_q \tag{1}$$

$$\frac{di_q}{dt} = \frac{v_q}{L_q} - \frac{R}{L_q}i_q - p\omega_r \frac{L_d}{L_q}i_d - p\omega_r \frac{\phi_m}{L_q} \tag{2}$$

$$\frac{d\omega_r}{dt} = \frac{3p\phi_m}{2J}i_q + \frac{3p}{2J}(L_q - L_d)i_d i_q - \frac{\beta}{J}\omega_r - \frac{\tau}{J} \tag{3}$$

with direct and quadrature axis currents i_d, i_q, shaft rotational velocity ω_r, direct and quadrature axis inductances L_d, L_q, stator resistance R, number of magnetic pole pairs p, magnetic flux ϕ_m, damping coefficient β, load torque τ, and rotor moment of inertia J. Note that the PMSM is a multi-input single-output system with inputs v_d and v_q and the output defined as the mechanical rotor velocity ω_r.

While the control methodology proposed in the following sections of this paper can be trivially extended to incorporate the generalized motor model given by (1)–(3), the motor used in our application has a salient isotropic rotor which renders the direct and quadrature inductances equal and simplifies the dynamics to

$$\frac{di_d}{dt} = \frac{v_d}{L} - \frac{R}{L}i_d + p\omega_r i_q \tag{4}$$

$$\frac{di_q}{dt} = \frac{v_q}{L} - \frac{R}{L}i_q - p\omega_r i_d - p\omega_r \frac{\phi_m}{L} \tag{5}$$

$$\frac{d\omega_r}{dt} = \frac{3p\phi_m}{2J}i_q - \frac{\beta}{J}\omega_r - \frac{\tau}{J}. \tag{6}$$

In order to drive the closed-loop system to the origin, we define the state errors as

$$\tilde{\omega}_r = \omega_r - \omega_r^* \tag{7}$$

$$\tilde{i}_d = i_d - i_d^* \tag{8}$$

$$\tilde{i}_q = i_q - i_q^* \tag{9}$$

where ω_r^* is the desired mechanical rotor speed and i_d^*, i_q^* are the target currents to be derived in the next section.

In addition, we also introduce a speed error integral term $\tilde{\theta}_r$, related to the speed error by $(d\tilde{\theta}_r/dt) = \tilde{\omega}_r$, to provide zero steady-state error despite an unknown load torque and damping coefficient. The complete error dynamic system used for control design is now given as

$$\frac{d\tilde{i}_d}{dt} = \frac{v_d}{L} - \frac{R}{L}i_d + p\omega_r i_q - \frac{di_d^*}{dt} \tag{10}$$

$$\frac{d\tilde{i}_q}{dt} = \frac{v_q}{L} - \frac{R}{L}i_q - p\omega_r i_d - p\omega_r \frac{\phi_m}{L} - \frac{di_q^*}{dt} \tag{11}$$

$$\frac{d\tilde{\omega}_r}{dt} = \frac{3p\phi_m}{2J}i_q - \frac{\beta}{J}\omega_r - \frac{\tau}{J} - \frac{d\omega_r^*}{dt} \tag{12}$$

$$\frac{d\tilde{\theta}_r}{dt} = \tilde{\omega}_r. \tag{13}$$

III. Continuous Space-Time Speed Controller via Integrator Backstepping

A. Stabilization of the Mechanical Subsystem

We begin our control design by introducing a CLF based solely on the output of the mechanical subsystem (12), (13) defined as

$$V_1 = \tfrac{1}{2}\tilde{\omega}_r^2 + \tfrac{1}{2}K_{\theta_r}\tilde{\theta}_r^2 \tag{14}$$

where K_{θ_r} is a positive design gain. Evaluating the time derivative of V_1 along the trajectories of the state using the chain rule yields the following expression:

$$
\begin{aligned}
\dot{V}_1 &= \tilde{\omega}_r \frac{d\tilde{\omega}_r}{dt} + K_{\theta_r}\tilde{\theta}_r \frac{d\tilde{\theta}_r}{dt} \\
&= \tilde{\omega}_r \left[\frac{3p\phi_m}{2J}i_q - \frac{\beta}{J}\omega_r - \frac{\tau}{J} - \frac{d\omega_r^*}{dt} + K_{\theta_r}\tilde{\theta}_r \right].
\end{aligned}
\tag{15}
$$

Focusing on the regulation of the state errors to zero, we assume constant or slowly varying reference signals, rendering $(d\omega_r^*/dt) = 0$. Because the inputs to the system are not available at the output, we treat i_q as a virtual input to the motor speed dynamics and backstep through an integrator into the electrical dynamics governing the torque-producing currents. Introducing an additional design gain $K_{\omega_r} \geqslant 0$, and choosing the stabilizing function i_q^* as

$$i_q^* = \frac{-K_{\omega_r}\tilde{\omega}_r + \frac{\beta}{J}(\tilde{\omega}_r + \omega_r^*) + \frac{\tau}{J} - K_{\theta_r}\tilde{\theta}_r}{\frac{3p}{2J}\phi_m} \tag{16}$$

will render the mechanical subsystem stable about the origin. This is seen by substituting i_q^* for i_q in (15) and evaluating $\dot{V}_1$

$$\dot{V}_1 = -K_{\omega_r}\tilde{\omega}_r^2 \leqslant 0. \tag{17}$$

While the above expression is only negative semidefinite, upon completion of the backstepping procedure, we will show that the closed-loop system is globally exponentially stable.

B. Stabilization of the Electrical Subsystem

The backstepping procedure has been used to ensure that the actual control inputs v_d and v_q drive the speed error to zero. We are now able to extend the CLF (18), (19) by including states $\tilde{i}_q$ and $\tilde{i}_d$

$$V_2 = V_1 + \tfrac{1}{2}K_q\tilde{i}_q^2 + \tfrac{1}{2}K_d\tilde{i}_d^2 \tag{18}$$

$$\dot{V}_2 = \dot{V}_1 + K_q\tilde{i}_q \frac{d\tilde{i}_q}{dt} + K_d\tilde{i}_d \frac{d\tilde{i}_d}{dt}. \tag{19}$$

In order to express the derivative of the quadrature current error $(d\tilde{i}_q/dt) = (di_q/dt) - (di_q^*/dt)$, (16) is differentiated as follows:

$$\frac{di_q^*}{dt} = \frac{(-K_{\omega_r} + \frac{\beta}{J})\dot{\tilde{\omega}}_r - K_{\theta_r}\tilde{\omega}_r}{\frac{3p}{2J}\phi_m}. \tag{20}$$

The derivative of the direct current $(d\tilde{i}_d/dt)$ is considerably simpler to express after noting that

$$i_d^* = \frac{di_d^*}{dt} = 0 \tag{21}$$

which implies

$$\tilde{i}_d = i_d \tag{22}$$

$$\frac{d\tilde{i}_d}{dt} = \frac{di_d}{dt} \tag{23}$$

since the direct component of the current produces no torque and is not needed to magnetize the rotor in a PMSM. However, the direct component can be easily made nonzero without loss of generality to allow for field weakening if a boost in top speed at the expense of torque is desired.

Expanding (20) with the dynamics given in (12) and substituting it into (10), we arrive at a transformed system in terms of state errors suitable for evaluating the total time derivative of the extended CLF (19)

$$\frac{d\tilde{i}_d}{dt} = \frac{v_d}{L} - \frac{R}{L}\tilde{i}_d + p(\tilde{\omega}_r + \omega_r^*)\left(\tilde{i}_q + i_q^*\right) \tag{24}$$

$$
\begin{aligned}
\frac{d\tilde{i}_q}{dt} &= \frac{v_q}{L} - \frac{R}{L}\left(\tilde{i}_q + i_q^*\right) \\
&\quad - p(\tilde{\omega}_r + \omega_r^*)\left(\tilde{i}_d + \frac{\phi_m}{L}\right) + \frac{2JK_\theta\tilde{\omega}_r}{3p\phi_m} \\
&\quad - \frac{2J}{3p\phi_m}\left((K_{\omega_r}\tilde{\omega}_r + K_\theta\tilde{\theta} - \frac{3p\phi_m}{2J}\tilde{i}_q)(K_{\omega_r} - \frac{\beta}{J})\right)
\end{aligned}
\tag{25}
$$

$$\frac{d\tilde{\omega}_r}{dt} = \frac{3p\phi_m}{2J}\tilde{i}_q - K_{\omega_r}\tilde{\omega}_r - K_{\theta_r}\tilde{\theta}_r \tag{26}$$

$$\frac{d\tilde{\theta}_r}{dt} = \tilde{\omega}_r. \tag{27}$$

Using these governing differential equations, we repeat the process performed in Section III-A by evaluating (19) and selecting the control inputs v_d and v_q that ensure $\dot{V}_2$ is negative definite. By substituting (24) and (25) into (19), we can choose our control inputs so that they cancel out all positive and indefinite terms while leaving useful negative definite terms that provide damping. If v_q and v_d are chosen as

$$v_q = -K_q\tilde{i}_q + Ri_q^* + p\omega_r\left(L\tilde{i}_d + \phi_m\right) + L\left(\frac{di_q^*}{dt} - \frac{3p\phi_m\tilde{\omega}_r}{2K_qJ}\right) \tag{28}$$

$$v_d = -K_d\tilde{i}_d - Lp\omega_r i_q^* - L\tilde{i}_q p\omega_r \tag{29}$$

the resulting closed loop error system is

$$\frac{d\tilde{i}_d}{dt} = -\left(\frac{K_d + R}{L}\right)\tilde{i}_d \tag{30}$$

$$\frac{d\tilde{i}_q}{dt} = -\left(\frac{K_q + R}{L}\right)\tilde{i}_q - \frac{3p\phi_m\tilde{\omega}_r}{2K_qJ} \tag{31}$$

$$\frac{d\tilde{\omega}_r}{dt} = \frac{3p\phi_m}{2J}\tilde{i}_q - K_{\omega_r}\tilde{\omega}_r - K_{\theta_r}\tilde{\theta}_r \tag{32}$$

$$\frac{d\tilde{\theta}_r}{dt} = \tilde{\omega}_r. \tag{33}$$

Using (30)–(33) to evaluate (19) shows

$$\dot{V}_2 = -K_{\omega_r}\tilde{\omega}_r^2 - \left(\frac{K_q + R}{L}\right)\tilde{i}_q^2 - \left(\frac{K_d + R}{L}\right)\tilde{i}_d^2 \tag{34}$$

is only negative semidefinite since the state $\tilde{\theta}_r$ has been cancelled out by the control inputs. To prove asymptotic
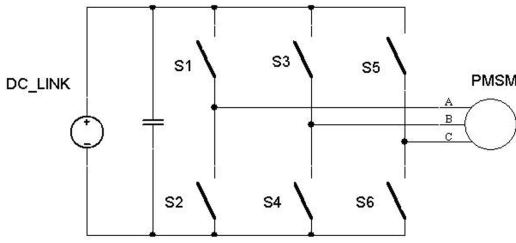
Fig. 1. Generalized architecture of a two-level power inverter.

Fig. 2. Quantized input space of a two-level power inverter in the stationary reference frame.

stability, note that V_2 is radially unbounded and observe that

$$\dot{V}_2 = 0 \rightarrow \tilde{i}_d = \frac{d\tilde{i}_d}{dt} = \tilde{i}_q = \frac{d\tilde{i}_q}{dt} = \tilde{\omega}_r = \dot{\tilde{\omega}}_r = 0. \quad (35)$$

Evaluating (32) at $\dot{V}_2 = 0$ results in the expression

$$0 = -K_{\theta_r}\tilde{\theta}_r. \quad (36)$$

Therefore, since no solution can stay identically in the set $S = \{[\tilde{i}_d, \tilde{i}_q, \tilde{\omega}_r, \tilde{\theta}_r]^T \,|\, \dot{V}_2 = 0\}$ other than the trivial solution, and observing that the error dynamic system (24)–(27) is autonomous as it is only dependent on the initial conditions, by the theorem of Barbashin and Krasovskii [33] the origin is globally asymptotically stable. Furthermore, because the closed-loop error system (30)–(33) is linear, the origin is in fact globally exponentially stable.

IV. POWER INVERTERS AND QUANTIZED-INPUT VOLTAGE REALIZATION

A. Two-Level Power Inverter

With a continuous control law at hand, we now address the problem of impressing these desired input voltages given a small discrete set of realizable commands. Input voltages to the motor drive are realized by selecting the switching configuration of a two-level power inverter, whose generalized architecture is shown in Fig. 1. The inverter consists of three half bridges connected in parallel, with each half bridge containing a high-side and low-side complementary pair of switches. Because the high-side and low-side switches can never be active at the same time, the inverter can be fully described by a binary ordered triple indicating the position of the high-side switch for each inverter leg. Given three legs, each being in one of two positions, there are a total of 2^3 possible configurations available as inputs to the motor with two of the configurations [111] and [000] both applying zero line-to-line voltage. The collective on/off status of the individual switches will be from here on referred to as the "switching state" in order to remain consistent with the current literature, though it should be noted that this is not truly a state of the system as it has no memory.

B. Overview of the SVM Algorithm

A fundamental issue in motor control design concerns bridging the gap between the continuous-valued inputs desired by the motor and the small finite set of seven unique inputs that are capable of being generated by a two-level inverter. Because the method we present is in the class of vector controls, it
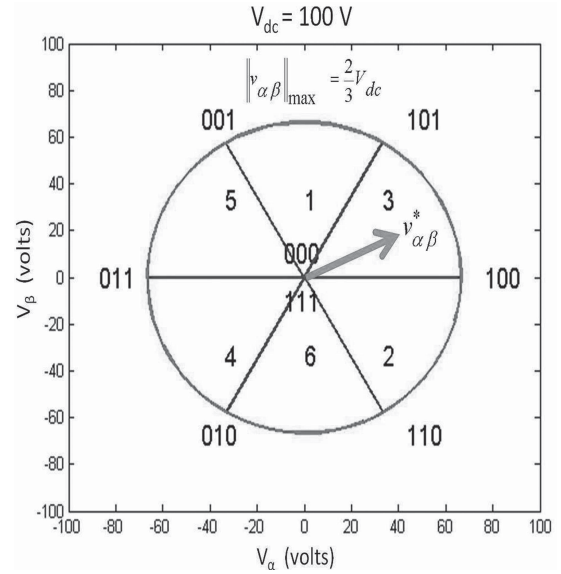
is insightful to describe how other algorithms in this class address this issue. Possibly the most popular algorithm used in modern motor control research to approximate continuous-valued input commands is SVM due to its relative simplicity, single switch event per commutation, and higher line-to-line voltage capability when compared to traditional ST-PWM [34]. SVM is a method of state-space averaging, where the duty cycles of realizable switching states bounding the desired reference input are computed such that the average on-times of the switching states average to the continuous-valued input. Fig. 2 shows the available states of a two-level inverter in the stationary reference frame with $\theta = 0$, along with a desired space vector with coordinates $v_{\alpha,\beta}^* = (v_\alpha^*, v_\beta^*)$. A fast average time-based convex combination of the input sequence to approximate the continuous input depicted in Fig. 2 is given by

$$(v_\alpha^*, v_\beta^*) \approx \frac{T_s - \eta - \gamma}{2}[000] \\ + \eta[100] + \gamma[101] \\ + \frac{T_s - \eta - \gamma}{2}[111] \quad (37)$$

where T_s is the sampling frequency and η, γ are the duty cycles assigned to each nonzero switching state and must satisfy $\eta, \gamma \geq 0$ and $\eta + \gamma \leq T_s$. It should be noted that other equivalent sequences exist, including those that only use a single zero vector for what is known as discontinuous PWM [34]. However, all the different variants of SVM involve fast switching between the two nonzero states that bound the desired input to approximate the command angle and switching to either one or both zero states to approximate the command magnitude. Typical FOC methods compute input commands in the synchronously rotating dq frame and use nested PI controllers for regulation of phase currents and rotor speed. In this reference frame, the synchronous motor behaves like a dc motor where nonsinusoidal reference inputs improve the quality of integral action on the steady-state error [2]. Once

the inputs v_q and v_d are calculated, they are rotated back into the stationary two-phase reference frame by the inverse Park transform, resulting in v_α and v_β. With the stationary reference frame mapped to the switching states of the inverter, the sector that bounds the input is computed to determine which three switching states to modulate.

C. Two-Level Inverter in the Synchronous Reference Frame

Rather than rotating a *dq* command onto a stationary inverter map, we find it more convenient to rotate the inverter map and therefore pose the entire inverter–motor system in a synchronous reference frame. Given a switching state

$$S = [S_a, S_b, S_c]^T \tag{38}$$

$$S_i \in \{0, 1\} \tag{39}$$

the phase-to-ground voltages for a two level inverter can be represented as

$$[v_{ag}, v_{bg}, v_{cg}]^T = V_{dc}S. \tag{40}$$

Assuming a wye connected motor, the phase to neutral voltages can be computed as

$$\begin{bmatrix} v_{an} \\ v_{bn} \\ v_{cn} \end{bmatrix} = \frac{1}{3} \begin{bmatrix} 2 & -1 & -1 \\ -1 & 2 & -1 \\ -1 & -1 & 2 \end{bmatrix} \begin{bmatrix} v_{ag} \\ v_{bg} \\ v_{cg} \end{bmatrix}. \tag{41}$$

With knowledge of the electrical angle of the rotor θ_e, the phase to neutral voltages are rotated into the synchronous reference frame with the Park transform as follows [2], [35]:

$$\begin{bmatrix} v_{qn} \\ v_{dn} \\ v_{0n} \end{bmatrix} = \frac{2}{3} \begin{bmatrix} \cos(\theta_e) & \cos\left(\theta_e - \frac{2\pi}{3}\right) & \cos\left(\theta_e + \frac{2\pi}{3}\right) \\ \sin(\theta_e) & \sin\left(\theta_e - \frac{2\pi}{3}\right) & \sin\left(\theta_e + \frac{2\pi}{3}\right) \\ \frac{1}{2} & \frac{1}{2} & \frac{1}{2} \end{bmatrix} \begin{bmatrix} v_{an} \\ v_{bn} \\ v_{cn} \end{bmatrix}. \tag{42}$$

V. STABILIZATION WITH QUANTIZED INPUTS

It is well known that, if a stable convex combination of unstable systems exists, then there exists a stabilizing switching rule between the systems [36]. An often nontrivial task noted in [36] is finding such a convex combination. We will show that the control law derived in Section III can be expressed as a stable convex combination of realizable inputs. Moreover, explicitly computing the control inputs given by (28) and (29) is unnecessary, as simply knowing the convex combination exists is enough formulate a switching rule that preserves the stability guarantees given by the continuous case.

Lemma 5.1: Denoting the state vector $x = [\tilde{i}_d, \tilde{i}_q, \tilde{\omega}_r, \tilde{\theta}_r]^T$ and input vector $[v_d(x), v_q(x)]^T = v_{dq}(x)$ satisfying the feasibility requirement that $|v_{dq}(x)| \leq (2/3)V_{dc}$, expressing the dynamic system defined by (24)–(27) as

$$\dot{x} = F(x) + G(x) v_{dq}(x) \tag{43}$$

define a Lyapunov function as in (18) by

$$V(x) = \frac{1}{2}Kx^2 \tag{44}$$

with weighting matrix K defined as

$$K = \text{diag}\left[K_d, K_q, 1, K_{\theta_r}\right]. \tag{45}$$

Suppose for all feasible x there exists $v_{dq}^*(x)$ such that

$$\frac{\partial V(x)}{\partial x}\left(F(x) + G(x)v_{dq}^*(x)\right) \leq 0. \tag{46}$$

Given discrete input pairs v_{dq}^k with $k = 0, 1, \ldots, 6$ corresponding to the seven unique realizable two-level inverter voltages, the quantized-input CLF derivative

$$\frac{\partial V(x)}{\partial x}\left(F(x) + G(x)v_{dq}^k\right) \tag{47}$$

satisfies

$$\min_k \frac{\partial V(x)}{\partial x}\left(F(x) + G(x)v_{dq}^k\right) \leq 0 \tag{48}$$

$$\forall \, x : |v_{dq}^*(x)| \leq \frac{2}{3}V_{dc}.$$

Proof: As illustrated in Fig. 2, any reference vector $v_{dq}^*(x)$ within the region of feasibility (having magnitude less than $(2/3)V_{dc}$) is contained within one of the six nonzero switching sectors of width $(\pi/3)$ with vertices (v_d^0, v_q^0), (v_d^i, v_q^i), (v_d^j, v_q^j), where $i, j \in \{1, 2, \ldots, 6\}$ are the nonzero switching states to the left and right of the reference vector and (v_d^0, v_q^0) is one of the two zero vectors. Containment within a switching sector ensures the existence of coefficients γ, η satisfying $\gamma, \eta \geq 0$, $\gamma + \eta \leq 1$ such that the reference vector is expressible as a convex combination of the realizable inputs, given by

$$v_{dq}^*(x) = \gamma v_{dq}^i + \eta v_{dq}^j + (1 - \gamma - \eta)v_{dq}^0. \tag{49}$$

Plugging (49) into (46) and noting that the system is control affine, we see that

$$\frac{\partial V(x)}{\partial x}\left(F(x) + G(x)v_{dq}^*(x)\right)$$
$$= \frac{\partial V(x)}{\partial x}\left(F(x) + G(x)\left(\gamma v_{dq}^i + \eta v_{dq}^j + (1 - \gamma - \eta)v_{dq}^0\right)\right)$$
$$= \gamma \frac{\partial V(x)}{\partial x}\left(F(x) + G(x)v_{dq}^i\right) + \eta\frac{\partial V(x)}{\partial x}\left(F(x) + G(x)v_{dq}^j\right)$$
$$+ (1 - \gamma - \eta)\frac{\partial V(x)}{\partial x}\left(F(x) + G(x)v_{dq}^0\right)$$
$$\leq 0. \tag{50}$$

Because γ, η, and $(1 - \gamma - \eta)$ are all nonnegative, (50) implies that at least one of the following inequalities holds:

$$\frac{\partial V(x)}{\partial x}\left(F(x) + G(x)v_{dq}^i\right) \leq 0 \tag{51}$$

$$\frac{\partial V(x)}{\partial x}\left(F(x) + G(x)v_{dq}^j\right) \leq 0 \tag{52}$$

$$\frac{\partial V(x)}{\partial x}\left(F(x) + G(x)v_{dq}^0\right) \leq 0 \tag{53}$$

which completes the proof of the lemma. ∎

A. Control Law

A block diagram of the proposed control method is given in Fig. 3. With Lemma 5.1 in hand, we are now able to define numerous input selection methods to optimize some performance metris while maintaining stability guarantees provided by the continuous Lyapunov methods from Section III so long as a sufficiently fast evaluation of the quantized input
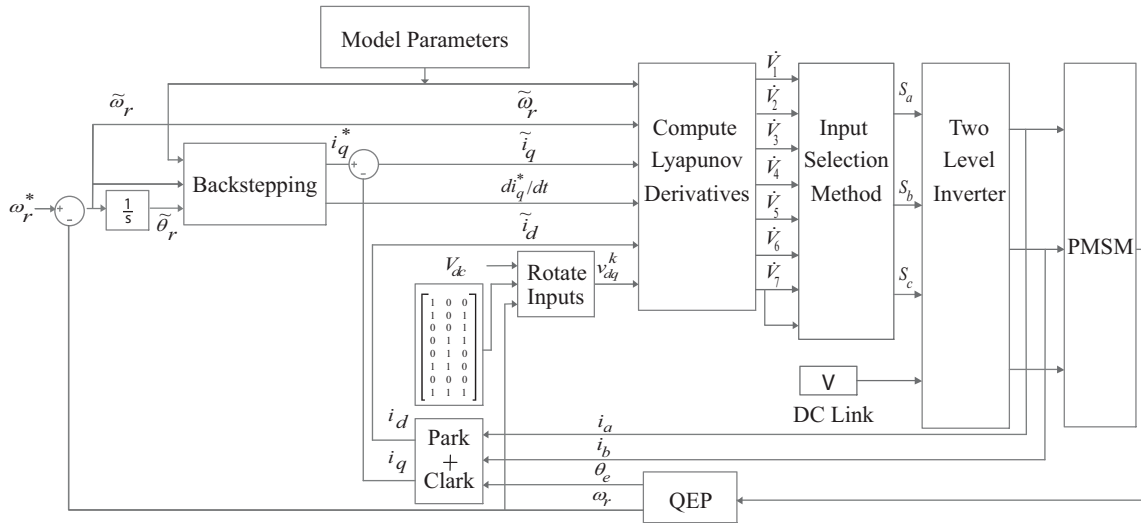
Fig. 3.   Block diagram of the proposed control method.

stability function given by (47) is possible for each input candidate. While the proof given above asserts that at least one of the three inputs bounding a stabilizing reference vector are themselves stabilizing, we will see in Section VI that other inputs not bounding the reference can also be stabilizing and can be used in the optimization of the switching sequence. For example, it is possible to penalize switching events by selecting the input state that results in the most negative value of the stability function and monitor the degree of stability this input provides as the motor evolves in time without performing any additional switching or optimization. As the stability function approaches zero and the motor becomes marginally stable, re-minimize (47) over k by selecting the input that again yields the most negative result. In this fashion, switching only occurs when it is necessary, i.e., only when stability would otherwise be lost if a new input was not selected. The step-by-step description of a minimum switching control law is given as follows, where for notational brevity, the quantized input stability function is denoted as $\dot{V}^k$.

1) Measure the state of the motor and express in the synchronous frame $\omega_r, \theta_r, i_d, i_q$.
2) Following the procedure outlined in Section III, compute $\tilde{\omega}_r, \tilde{\theta}_r, i_q^*, (di_q^*/dt)$.
3) Use the measured electrical angle $\theta_e = p\theta_r$ and (42) to express the seven unique input voltages in the synchronous frame.
4) Use the dynamics of the system given by (24)–(27) to evaluate all seven values of the stability function $\dot{V}^k$.
5) Select input k that satisfies

$$\min_{k} \dot{V}^k \leq 0.$$

   Because of Lemma 5.1, we know that at any instant at least one of the input states will produce a negative-valued stability function.
6) Without switching, continue to measure the state and update the value of $\dot{V}^k$ until stability would be lost if a switching event does not occur.
7) Re-evaluate the stability function and again choose the minimizing input.

One point worth noting is that this algorithm is optimal in the sense that it minimizes the average switching frequency under stability constraints so long as the evaluation of the stability function is much faster than the electrical time constant of the motor. Other control laws can be formulated that leverage the stabilizing effect of each input in order to optimize other metrics, such as minimizing torque ripple, maximizing torque response, or minimizing (dV/dt) stress on the inverter.

VI. SIMULATION RESULTS

The motor–inverter system was simulated in MATLAB with continuous dynamics given in (4) computed using a classical Runge–Kutta (RK4) integrator with a time step equal to 10 times the control frequency. Measurements are simulated by adding Gaussian noise to the states evolved by the RK4 method and are subsequently marched forward by one time step corresponding to the control period. These state prediction estimates are used along with the closed-form expressions of $i_q^*, (di_q^*/dt)$, and the model dynamics to estimate the stability function $\dot{V}^k, k = 0, 1, \ldots, 7$ at the next control period to allow for a switching decision before stability is lost. The initial model parameters are given in Table I.

While the step response and corresponding current dynamics given in Fig. 5 show good speed regulation performance, a perhaps more insightful evaluation of the controller is performed by plotting the values of the stability function $\dot{V}^k$ over all inputs while denoting the actual switching sequence selected by the control law as a means of showing what the stability of the system would be at a given time for each input had that input been selected. Fig. 4(a) shows the stabilizing effect of each input as the motor just begins to rotate from rest, where for readability purposes every 50th decision instance has been designated with a marker. At time $t = 0$, the controller is initialized to state 000, which immediately loses stability as the errors begin to increase. The controller then selects input 100 as the best input and remains there for quite some time as the inertia of the motor is overcome, and during this period approximately 500 switching events are skipped. This demonstrates a very intuitive

TABLE I
MOTOR PARAMETERS AND CONTROL GAINS USED FOR SIMULATION

Symbol	Value	Description
p	9	Pole pairs
L	8.0 mH	Stator inductance per phase
R	2.0 mΩ	Stator resistance per phase
J	1 kgm^2	Rotor moment of inertia
β	0.5 Nm.s/rad	Viscous damping coefficient
τ	25 Nm	External load torque
ϕ	0.44 Nm/A	Magnetic flux
K_{ω_r}	1	Speed error gain
K_{θ_r}	10	Speed error integrator gain
K_q	1	Quadrature current error gain
K_d	0.75	Quadrature current error gain
V_{dc}	200 V	DC link voltage
f_s	10 kHz	Maximum switching frequency

behavior of the control law; it does not switch away from the input that generates the most torque when acceleration is required.

Continuing with this method of evaluating the control law, Fig. 4(b) shows the selection process of the input sequence after the initial input no longer provides stability. Given the current state of the motor over the time interval shown, the inverter input 110 is stabilizing with exception of four instances where switching occurs. Referring to Fig. 4, consider time $t = 0.4958 = t_0$ s. The controller applies the input 010 for the next four decision instances after which it predicts that remaining at 010 will yield instability at the next step and thus switches to a new input. This input is predicted to make the value of the stability function positive in the next time step so the controller again selects 010. Over the next six time steps $t_0+4\Delta T$ through $t_0+9\Delta T$, this input remains stabilizing and therefore no switching occurs, allowing the stability function to be evaluated using only the current input. However, at $t_0+10\Delta T$, the stability function at time $t_0+11\Delta T$ is predicted to become positive. At this point, the stability function is again minimized and a new input is selected as it yields the minimizing value. This input is again determined to be stabilizing for one time step, where again input 010 is selected for six more time steps before further switching becomes necessary. This behavior is not always periodic as can be seen at $t = 0.497$ s. At this point, the state 011 is stabilizing by a small margin yet is predicted to maintain stability for 14 time steps. The advantage of this method is that switching is only occurring when it is necessary from a stability viewpoint. After an input k is selected, we simply follow $\dot{V}^k$ to zero before making another selection, allowing for the reduction in switching losses without prohibiting fast switching when it is required, as is typical of static switching frequency methods. Additionally, the control law randomizes the switching pattern to an extent. While switching at a nonuniform minimum average frequency can increase torque ripple and total acoustic noise, spreading out the spectral content by decreasing coherency can be useful in certain applications such as reducing the detectability of a submersible vehicle motor drive without employing noise injection techniques used in random PWM methods [21], [23].
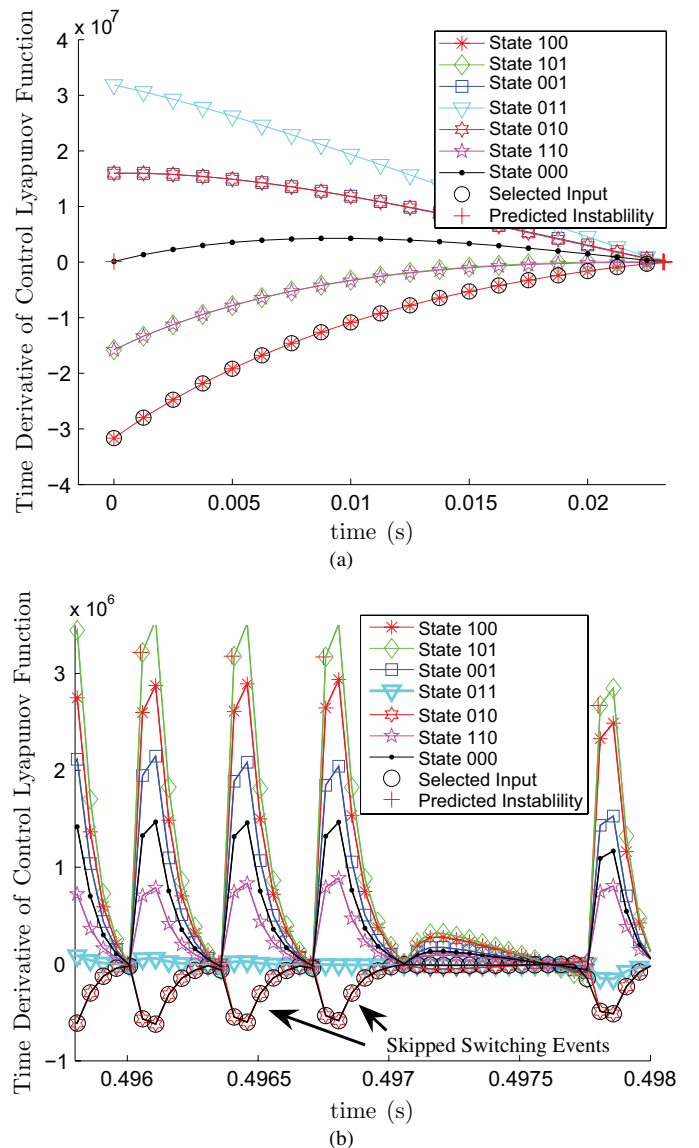

Fig. 4. Simulation results depicting the input selection process. (a) Stabilizing effect of each input as the motor accelerates. Initially at rest with $\theta = 0$ aligned with $I_{\text{phase} A} = I_q$, the switching state producing the maximal torque is selected (100). Note that the two other nonzero states (101 and 110), where phase A is connected to V_{dc}, are also stabilizing but to a lesser extent and produce the same value of the stability metric, shown drawn on top of each other as the second curve from the bottom of the plot. Additionally, the two states (001 and 010) with phase A connected to ground and one other phase connected to V_{dc} are not stabilizing and also produce identical stability curves, shown as the second curve from the top. Finally, the topmost curve verifies the intuition that the most unstable switching choice 011 is the opposite (largest distance in the $\mathcal{L}_1$ sense) switching state of the most stabilizing choice. (b) Switching sequence selection based on predicted stability. At each time step, the value of the CLF is computed for each input, representing the stabilizing effect on the system had that input been selected.

VII. EXPERIMENTAL RESULTS

A. Description of the Experimental Testbed

The experimental test bed shown in Fig. 6 has been designed to verify the effectiveness of the proposed control law. The algorithm depicted by Fig. 3 has been developed in Simulink and implemented in real time on dSpace hardware through the real time workshop software package available from MathWorks. The modular DS1006 system from dSpace
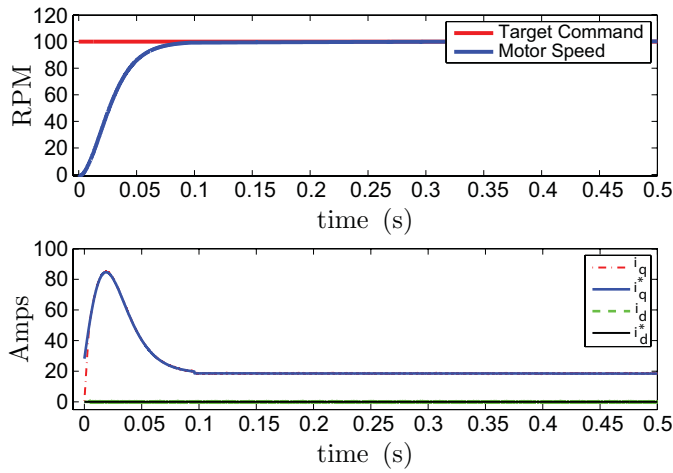
Fig. 5. Simulation of speed and current given a 100 r/min step command with known parameters.

TABLE II
MODEL PARAMETERS AND CONTROL GAINS USED FOR EXPERIMENTAL RESULTS

| Symbol	Value	Description
p	5	pole pairs
L	2.8 mH	Stator inductance per phase
R	20 mΩ	Stator resistance per phase
J	0.69 kgm^2	Rotor moment of inertia
β	0.1763 Nm.s/rad	Viscous damping coefficient
τ	0 Nm	Estimated load torque
ϕ	0.08 Nm/A	Magnetic flux
$K_{\omega r}$	1	Speed error gain
$K_{\theta r}$	10	Speed error integrator gain
K_q	1	Quadrature current error gain
K_d	0.75	Quadrature current error gain
V_{dc}	100 V	DC link voltage
f_s	10 kHz	Maximum switching frequency
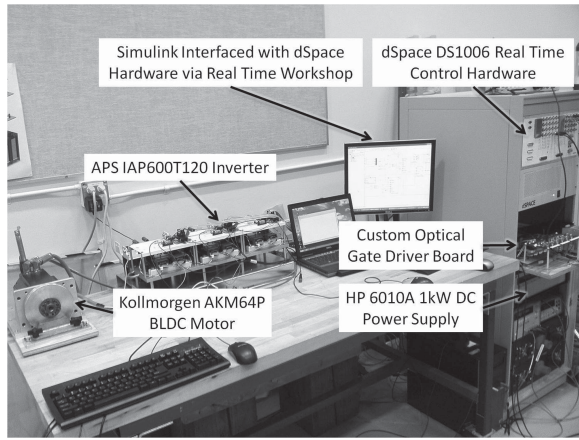
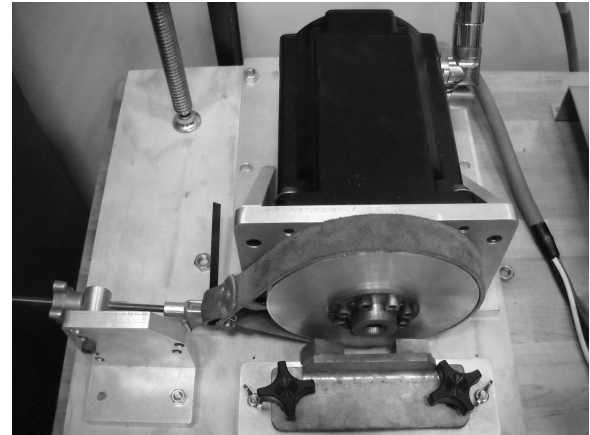Fig. 6. Testbed used for controller evaluation.

Fig. 7. Braking mechanisms used to provide a load to the motor. NdFeB magnets at the bottom of the figure serve as an eddy current brake while the leather strap provides frictional force proportional to the tension in the strap as well as to the direction of rotation.

has been augmented with the DS5202 FPGA base board equipped with the ACMC motor control card capable of PWM synchronized phase current and dc link measurements, position measurements from QEP encoder signals, and the generation of gate drive signals from 0%−100% duty cycle. Actuation is achieved with an IAPL600T120 900 V 600-A two-level inverter from Applied Power Systems optically connected to the ACMC through a custom-made laser gate driver board to minimize the coupling of electromagnetic noise and the drive signals. The inverter independently inserts a 5-μs deadtime between the high-side and low-side devices of each inverter leg as the corresponding phase transitions from high to low. This research was motivated by the desire to control high-current high-torque motors where the switching frequency is severely limited, which led us to a 540-kW inverter solution. However, initial experiments were conducted on a scaled-down bench-top Kollmorgen AKM64P five-pole-pair three-phase brushless servo motor. A viscous load is applied through a tension brake applied to an aluminum disk attached to the rotor as well as an eddy current magnetic brake used to apply load disturbances, which consists of a pair of NdFeB magnets attached to a plate that can be positioned at variable distances from the rotor disk. The load provided by both of these mechanisms, shown in Fig. 7 is unknown and allows the demonstration of the

controller's disturbance rejection capabilities and insensitivity to parametric uncertainty in the damping coefficient β as well as the load torque τ. Unless otherwise noted, the model parameters provided to the controller are given in Table II.

B. Results

We begin experimental verification of the proposed controller by applying a series of step commands over a variety of operating points without any applied load. As seen in Fig. 8, as the speed of the motor increases, faster switching is required to maintain speed regulation. While the data exhibits a small overshoot at the command transitions, the controller achieves rapid speed regulation despite the low switching frequency.

In addition to speed regulation, the ability to accurately control acceleration and deceleration is an important feature to be examined in the evaluation of a motor controller. While the stability proof presented in Section V assumes an autonomous system, which somewhat restricts our focus to the speed regulation problem, if a time-varying input is applied whose variations are slow compared to the dynamics of the system, the input commands will appear approximately
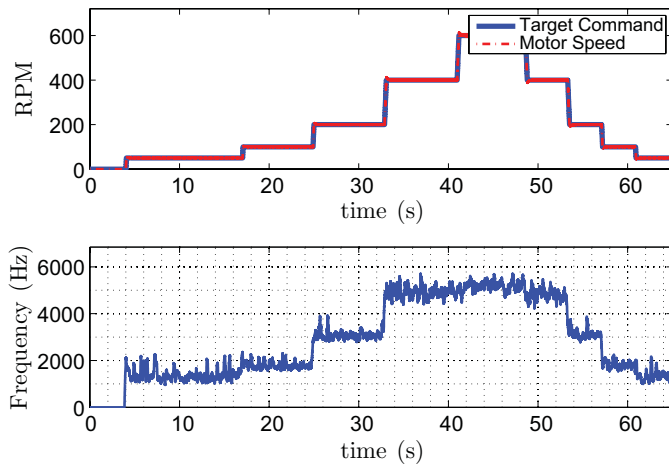
Fig. 8. Experimentally measured step response and average switching frequency for various speed commands. A window of 500 samples is used to determine the localized average switching frequency of each leg of the inverter, which is then averaged across all three legs. The variable switching frequency allowed by the input selection method increases as necessary with increasing speed, but the overall switching frequency remains relatively small.

constant and the theoretical stability analysis will hold. To investigate this further, a slowly varying sinusoidal input reference with $\omega_r^* = 300 \sin(0.5t)$ is used as a reference speed command, and a viscous load is applied to the rotor using the tension and eddy current braking mechanisms. The load is both unknown and asymmetric, as it applies a different amount of force in the clockwise and counterclockwise directions. Fig. 9 demonstrates the ability of the proposed control method to track slowly varying commands in both directions with an uncertain load while maintaining a very low switching frequency.

C. Robustness to Parametric Uncertainty

Another desirable attribute of a motor control system is robustness to parametric uncertainty. Sensitivity to parameters in model-based designs can greatly inhibit the implementation of the controller, particularly when the parameter count is high as is the case in our proposed method. While a rigorous analysis of the robustness to parametric uncertainty is beyond the scope of this paper, it is conceptually worthwhile to point out that the input selection algorithm discussed in Section V-A reduces the apparent parametric sensitivity by evaluating the stabilizing effect of each input using the same parameters for each evaluation. Because every parameter is intrinsically positive, parametric error in the electrical subsystem will only scale the values of $\dot{V}^k$ but will not change the ordering of the inputs in terms of which one is the most stabilizing. One caveat worth noting is that parametric error in the mechanical subsystem can influence controller performance, as mechanical parameters are used to determine the target reference current i_q^*. While this has been observed experimentally to add a small degree of overshoot to the response, the steady-state behavior remains unchanged because of the integral action incorporated into the mechanical component of the CLF. To demonstrate this robustness, four experiments were conducted where the values provided to the controller for the damping coefficient
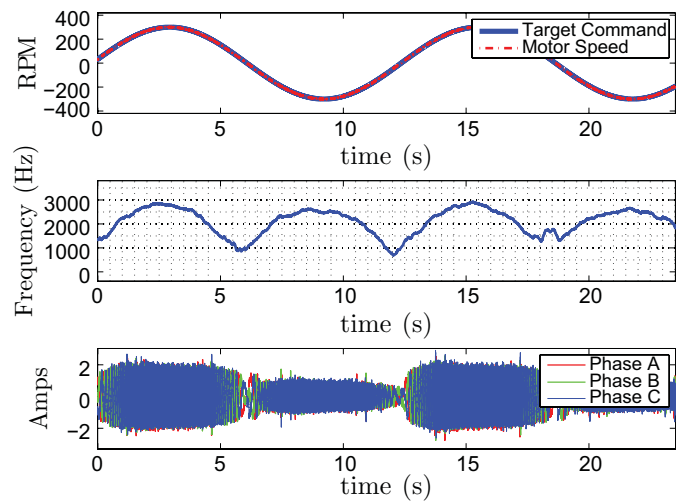

Fig. 9. Experimentally measured tracking of a sinusoidal speed reference. The motor controller is capable of accurate control of acceleration and deceleration while given an unknown asymmetric load. Similar to the step response data, the switching frequency increases with rotor speed as needed. However, it also increases with increased load. The envelope of the phase currents shows that positive (clockwise) rotation requires more torque to maintain speed tracking than negative rotation because of asymmetries in the braking mechanism. The peak switching frequency during positive rotation is 2930 Hz, while the peak switching frequency during negative rotation is 2628 Hz, a difference of about 300 Hz.
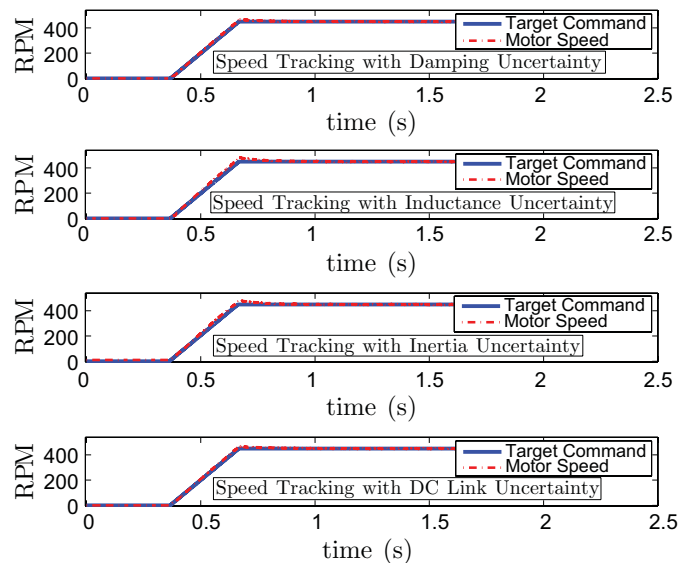

Fig. 10. Experimentally measured tracking performance with variations in model parameters.

β, the inductance L, the rotor moment of inertia J, and the dc link voltage V_{dc} were changed by a factor of two or more. The effects of this parametric variation are shown as a series of plots given in Fig. 10.

The first plot shows the tracking response with the inductance more than tripled from the nominal value, from 2.8 to 10 mH. This parameter is used in the evaluation of each input, and the net result on the performance of the controller is negligible. The next two plots show the effects of doubling the damping coefficient β from 0.1763 to 0.3526 Nm.s/rad and more than doubling the rotor moment of inertia J from 0.69 to 3 kgm^2. As these two parameters are part of the mechanical subsystem and influence the reference current i_q^* derived
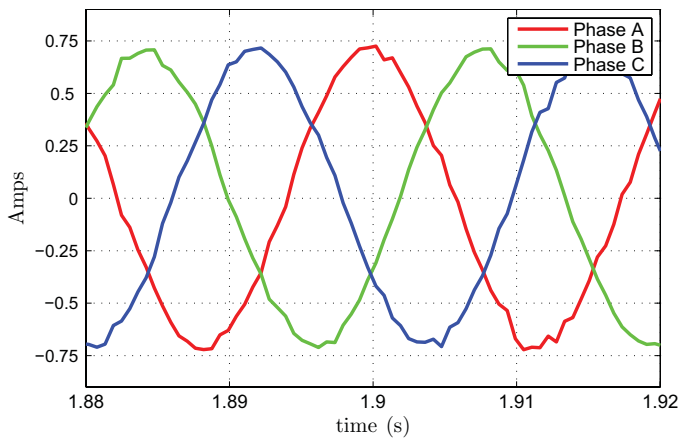
Fig. 11. Experimentally measured phase currents generated by the quantized input method controlling an unknown load at 500 r/min and a switching frequency of about 5 kHz.
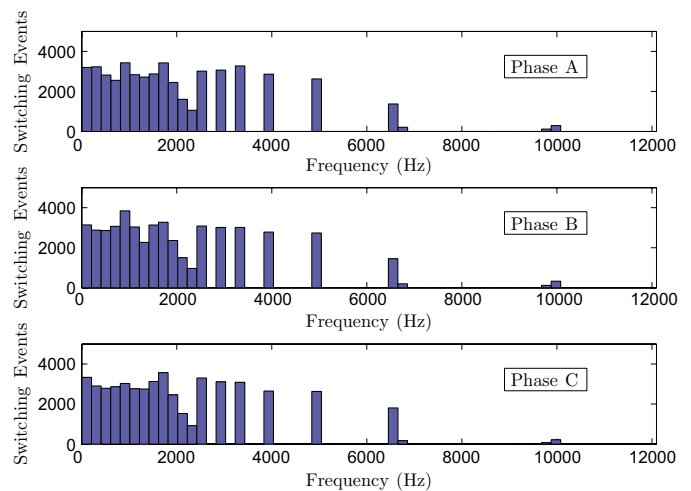

Fig. 12. Histogram derived from experimental data depicting how frequently the power electronic switching devices operate at different frequencies. The data shows an even distribution of actuator stress across each leg of the inverter.

from the backstepping procedure, parametric uncertainty β and J can contribute to adding overshoot to the response. However, these transient effects are short-lived because of the incorporation of integral action in the mechanical component of the CLF which allows the input selection method to adapt to mechanical parametric error. The last plot shows the response of the system when the dc link measurement is doubled from its actual value of 100 to 200 V. Similar to the parametric errors in the inductance, measurement errors in the dc link voltage have no effect on the system as it does not change the relative stabilizing effect of each input. It was found experimentally that, as long as the actual dc link voltage and current sourcing capability were sufficient to achieve the desired speed and torque, any overestimate of the dc link voltage had no effect on the controller, while an underestimate occasionally resulted degraded performance, likely due to the controller falsely determining that no inputs will provide the necessary amount of torque. This attribute can allow the elimination of a dc link sensor so long as a lower bound on the link voltage is known.

D. Performance and Actuator Longevity Issues That Can Arise Due to Nonconstant Switching Frequency

One of the features of fixed-frequency commutation strategies that differentiate them from variable-switching frequency techniques is their ability to generate approximately sinusoidal phase currents which in turn produce minimal torque ripple. Unlike variable-frequency controllers, such as DTC, that use hysteresis bands to control flux and torque as opposed to directly controlling the phase currents, the proposed controller incorporates a model of the motor to direct the minimum energy solution of the closed-loop system to the origin of the error dynamic system through the use of control Lyapunov functions and it is therefore plausible that the generated currents will more closely match the characteristic sinusoidal back EMF waveforms of the motor despite the variable switching frequency behavior. Fig. 11 verifies the controller's emergent capability to generate sinusoidal phase currents by allowing energy-related control Lyapunov functions to guide the input selection process.

Another advantage to SVM and other fixed-frequency commutation methods is that they yield the same degree of stress on each of the power electronic switching elements, which can contribute to greater actuator longevity. While variable switching frequency methods cannot guarantee this behavior, it is intuitive that a smoothly running motor with sinusoidal phase currents should equally employ each power electronic switch in the inverter. To verify this, the localized (100-point moving average) switching frequency of each leg of the inverter is used to generate a histogram detailing how often each switch operates at each frequency. This method of analysis is chosen over simply counting the total number of switching events per device because it is possible for a switching element to operate at a locally higher frequency than the remaining devices while being utilized comparatively less often than others at larger time scales, resulting in the false conclusion that the switching effort is balanced. Fig. 12 shows that the actuator stress is evenly distributed across each leg of the inverter at every frequency, implying that the low average switching frequency seen in Fig. 8 is not due to some inverter states rarely being selected, but is rather due to an even reduction in total switching events.

VIII. CONCLUSION

We presented a new method for closed-loop control of a motor–inverter system that utilizes the advantages of field orientation while accounting for the quantized input nature of the actuator with an energy-related commutation strategy directly built into the control law. The proposed controller uses model-based stability measures to compare each realizable input in a decision process designed to preserve stability while minimizing switching events. The control law generates a low switching frequency that naturally varies as demands on the motor change. Yet it is capable of producing sinusoidal phase currents and an even distribution of actuator stress, it is parametrically insensitive, and yields fast torque response while maintaining independent control of the torque and flux producing currents.

REFERENCES

[1] F. Blaschke, "The principle of field orientation as applied to the new transvector closed loop control for rotating field machines," *Siemens Rev.*, vol. 39, pp. 217–220, May 1972.

[2] P. C. Krause, O. Wasynczuk, and S. D. Sudhoff, *Analysis of Electric Machinery and Drive Systems*. Piscataway, NJ: IEEE Press, 2002.

[3] S. Li and Z. Liu, "Adaptive speed control for permanent-magnet synchronous motor system with variations of load inertia," *IEEE Trans. Ind. Electron.*, vol. 56, no. 8, pp. 3050–3059, Aug. 2009.

[4] J. Solsona, M. Valla, and C. Muravchik, "Nonlinear control of a permanent magnet synchronous motor with disturbance torque estimation," *IEEE Trans. Energy Convers.*, vol. 15, no. 2, pp. 163–168, Jun. 2000.

[5] L. Tao, W. Jiuhe, T. Yi, and W. Lei, "A new nonlinear control strategy for PMSM," in *Proc. Int. Conf. Comput. Design Appl.*, vol. 3. Jun. 2010, pp. 186–189.

[6] V. Petrovic, R. Ortega, A. Stankovic, and G. Tadmor, "Design and implementation of an adaptive controller for torque ripple minimization in PM synchronous motors," *IEEE Trans. Power Electron.*, vol. 15, no. 5, pp. 871–880, Sep. 2000.

[7] F. Aghili, M. Buehler, and J. Hollerbach, "Optimal commutation laws in the frequency domain for PM synchronous direct-drive motors," *IEEE Trans. Power Electron.*, vol. 15, no. 6, pp. 1056–1064, Nov. 2000.

[8] R. Marino, P. Tomei, and C. Verrelli, "Adaptive field-oriented control of synchronous motors with damping windings," *Eur. J. Control*, vol. 14, no. 3, pp. 177–196, 2008.

[9] M. Ouassaid, M. Cherkaoui, A. Nejmi, and M. Maarou, "Nonlinear torque control for PMSM: A Lyapunov technique," in *Proc. World Acad. Sci., Eng. Technol.*, vol. 6. Jun. 2005, pp. 118–121.

[10] M. Ouassaid, M. Cherkaoui, and Y. Zidani, "A nonlinear speed control for a PM synchronous motor using an adaptive backstepping control approach," in *Proc. IEEE Int. Conf. Ind. Technol.*, vol. 3. May 2004, pp. 1287–1292.

[11] M. Vilathgamuwa, M. Rahman, and K. Tseng, "Nonlinear control of interior permanent magnet synchronous motor," in *Proc. Ind. Appl. Conf.*, vol. 2. 2000, pp. 1115–1120.

[12] D. Dawson, J. Hu, and T. Burg, *Nonlinear Control of Electric Machinery*. New York: Marcel Dekker, 1998.

[13] D. Dawson, J. Carroll, and M. Schneider, "Integrator backstepping control of a brush DC motor turning a robotic load," *IEEE Trans. Control Syst. Technol.*, vol. 2, no. 3, pp. 233–244, Sep. 1994.

[14] Z. Cai, M. de Queiroz, and D. Dawson, "Robust adaptive asymptotic tracking of nonlinear systems with additive disturbance," *IEEE Trans. Autom. Control*, vol. 51, no. 3, pp. 524–529, Mar. 2006.

[15] T. Ghennam, E. Berkouk, and B. Francois, "A novel space-vector current control based on circular hysteresis areas of a three-phase neutral-point-clamped inverter," *IEEE Trans. Ind. Electron.*, vol. 57, no. 8, pp. 2669–2678, Aug. 2010.

[16] B. Vafakhah, J. Salmon, and A. Knight, "A new space-vector PWM with optimal switching selection for multilevel coupled inductor inverters," *IEEE Trans. Ind. Electron.*, vol. 57, no. 7, pp. 2354–2364, Jul. 2010.

[17] K. Basu, J. S. S. Prasad, G. Narayanan, H. K. Krishnamurthy, and R. Ayyanar, "Reduction of torque ripple in induction motor drives using an advanced hybrid PWM technique," *IEEE Trans. Ind. Electron.*, vol. 57, no. 6, pp. 2085–2091, Jun. 2010.

[18] F. Vargas-Merino, M. Meco-Gutierrez, J. Heredia-Larrubia, and A. Ruiz-Gonzalez, "Low switching PWM strategy using a carrier wave regulated by the slope of a trapezoidal modulator wave," *IEEE Trans. Ind. Electron.*, vol. 56, no. 6, pp. 2270–2274, Jun. 2009.

[19] E. Iyasere, E. Tatlicioglu, and D. Dawson, "Backstepping PWM control for maximum power tracking in photovoltaic array systems," in *Proc. Amer. Control Conf.*, Jul. 2010, pp. 3561–3565.

[20] A. Trzynadlowski, R. Kirlin, and S. Legowski, "Space vector PWM technique with minimum switching losses and a variable pulse rate [for VSI]," *IEEE Trans. Ind. Electron.*, vol. 44, no. 2, pp. 173–181, Apr. 1997.

[21] K. Borisov, T. Calvert, J. Kleppe, E. Martin, and A. Trzynadlowski, "Experimental investigation of a naval propulsion drive model with the PWM-based attenuation of the acoustic and electromagnetic noise," *IEEE Trans. Ind. Electron.*, vol. 53, no. 2, pp. 450–457, Apr. 2006.

[22] R. Kirlin, C. Lascu, and A. Trzynadlowski, "Shaping the noise spectrum in power electronic converters," *IEEE Trans. Ind. Electron.*, vol. 58, no. 7, pp. 2780–2788, Jul. 2011.

[23] Y.-C. Lim, S.-O. Wi, J.-N. Kim, and Y.-G. Jung, "A pseudorandom carrier modulation scheme," *IEEE Trans. Power Electron.*, vol. 25, no. 4, pp. 797–805, Apr. 2010.

[24] S. Underwood and I. Husain, "Online parameter estimation and adaptive control of permanent-magnet synchronous machines," *IEEE Trans. Ind. Electron.*, vol. 57, no. 7, pp. 2435–2443, Jul. 2010.

[25] I. Takahashi and T. Noguchi, "A new quick-response and high-efficiency control strategy of an induction motor," *IEEE Trans. Ind. Appl.*, vol. 22, no. 5, pp. 820–827, Sep. 1986.

[26] N. Farid, B. Sebti, K. Mebarka, and B. Tayeb, "Performance analysis of field-oriented control and direct torque control for sensorless induction motor drives," in *Proc. Medit. Conf. Control Autom.*, Jun. 2007, pp. 1–6.

[27] H. Le-Huy, "Comparison of field-oriented control and direct torque control for induction motor drives," in *Proc. 34th IAS Annu. Meeting Conf. Ind. Appl.*, vol. 2. 1999, pp. 1245–1252.

[28] J. Beerten, J. Verveckken, and J. Driesen, "Predictive direct torque control for flux and torque ripple reduction," *IEEE Trans. Ind. Electron.*, vol. 57, no. 1, pp. 404–412, Jan. 2010.

[29] B. Veselic, B. Perunicic-Drazenovic, and C. Milosavljevic, "Improved discrete-time sliding-mode position control using Euler velocity estimation," *IEEE Trans. Ind. Electron.*, vol. 57, no. 11, pp. 3840–3847, Nov. 2010.

[30] T. Geyer, G. Papafotiou, and M. Morari, "Model predictive direct torque control—Part I: Concept, algorithm, and analysis," *IEEE Trans. Ind. Electron.*, vol. 56, no. 6, pp. 1894–1905, Jun. 2009.

[31] J. Martinez, R. Kennel, and T. Geyer, "Model predictive direct current control," in *Proc. IEEE Int. Conf. Ind. Technol.*, Mar. 2010, pp. 1808–1813.

[32] C. Ortega, A. Arias, C. Caruana, J. Balcells, and G. M. Asher, "Improved waveform quality in the direct torque control of matrix-converter-fed PMSM drives," *IEEE Trans. Ind. Electron.*, vol. 57, no. 6, pp. 2101–2110, Jun. 2010.

[33] H. K. Khalil, *Nonlinear Systems*. Englewood Cliffs, NJ: Prentice-Hall, 2002.

[34] M. P. Kazmierkowski, R. Krishnan, and F. Blaabjerg, *Control in Power Electronics*. New York: Academic, 2002.

[35] K. Corzine, "Operation and design of multilevel inverters," Office of Naval Research, Univ. Missouri-Rolla, Dec. 2003, p. 52.

[36] D. Liberzon, *Switching in Systems and Control*. Basel, Switzerland: Birkhäuser, 2003.

Gideon Prior received the B.S. and M.S degrees in electrical engineering from the University of California, San Diego, in 2007 and 2009, respectively, where he is currently pursuing the Ph.D. degree in dynamic systems and control.

He has held internships with the Jet Propulsion Laboratory, SPAWAR Systems Center and is currently with a research and development group at General Atomics focused on developing new energy related technologies. His current research interests include switched input systems, power electronics, electric machinery, and energy conversion.

Mr. Prior is a McNair Scholar and a fellow of the Cymer Center for Control Systems and Dynamics.

Miroslav Krstic (S'92–M'95–SM'99–F'02) is an Associate Vice Chancellor for Research with the University of California, San Diego (UCSD), holds the Daniel L. Alspach Chair of Dynamic Systems and Control, and is the Founding Director of the Cymer Center for Control Systems and Dynamics, UCSD. He has held the Russell Severance Springer Distinguished Visiting Professorship with the University of California, Berkeley, and the Harold W. Sorenson Distinguished Professorship with the UCSD. He has co-authored nine books on adaptive, nonlinear, and stochastic control, extremum seeking, control of PDE systems including turbulent flows, and control of delay systems.

Prof. Krstic is a fellow of IFAC and serves as Senior Editor of the IEEE TRANSACTIONS ON AUTOMATIC CONTROL and *Automatica*. He was the Vice President of the IEEE Control Systems Society. He was a recipient of the PECASE, NSF Career, and ONR Young Investigator Awards, as well as the Axelby and Schuck Paper Prizes. He was the first recipient of the UCSD Research Award in engineering.